Published as: Kaci, M. , Dehouche, N. , Focke, W. W. and Merwe, E. M. (2019), A degradation study of polyamide 11/vermiculite nanocomposites under accelerated UV test. Polym Eng Sci. doi:10.1002/pen.25115

A Degradation Study of Polyamide 11/Vermiculite Nanocomposites under Accelerated UV Test

Mustapha Kaci[1], Nadjet Dehouche[1], Walter W. Focke[2], Elizabet M. van der Merwe[3]

[1]Laboratoire des Matériaux Polymères Avancés (LMPA), Université de Bejaia 06000, Algeria

[2]Institute of Applied Materials, Department of Chemical Engineering, University of Pretoria, South Africa

[3]Chemistry Department, University of Pretoria, South Africa

Abstract

Accelerated photooxidation under UV test of polyamide 11 (PA11) films filled with unmodified vermiculite (UMVC) clay at 5 wt % was investigated up to 600 h. Film samples of ~60 µm thick, were prepared by melt compounding using a cast extruder and exposed to UV light irradiation at λ>295 nm. FTIR spectra indicated similar structural changes occurring in both PA11 and PA11/UVMC nanocomposite along the photooxidation process, resulting in imides and carboxylic acids as the main carbonyl products. It was however observed that the formation rate of carbonyls in the PA11/UVMC nanocomposite was slower compared to neat PA11. This behavior is consistent with the yellowing index (YI) evolution determined by UV-vis spectroscopy. Further, the photooxidation stability of the samples was also evaluated by the onset oxidation temperature (OOT) determined by DSC. The results indicated a better stability of the nanocomposite film compared to neat PA11, corroborating well the data obtained by FTIR and UV-visible techniques.

Keywords: Photooxidation; polyamide 11; vermiculite; nanocomposites; degradation.

1. Introduction

PA11 is a bio-based engineering thermoplastic derived from a renewable resource (castor oil) [1]. It is biocompatible and has the advantage of being less hydrophilic than the commonly used polyamide-6 and polyamide-6,6 [2]. Moreover, the polymer offers excellent piezoelectric properties, a low wear and abrasion and high chemical resistance [3]. It is therefore widely used in a large range of fields from automotive to offshore applications [4], despite its low impact strength, tensile strength and thermal properties [5]. To further improve its properties, the addition of reinforcing nanofillers to PA11 is considered as one of the most efficient methods [6, 7]. Among nanofillers, clays can be classified depending either on their aspect ratio or on the organic modification for improving their compatibility with the polymer matrix. These aspects have a direct effect on the polymer-filler interactions, and subsequently on the properties of the materials. According to Macheca et al. [7], high particle aspect ratios are desirable and are achieved by extensive delamination and even exfoliation of clay flakes. These are favored by strong interfacial adhesion and appropriate mixing processes, resulting in a homogeneous dispersion of clay layers within the polymer matrix [7]. PA11-vermiculite nanocomposites have recently been the focus of a large number of studies [8-17]. These were mainly devoted to the preparation methods and characterization of the structure-property relationships with various nanofiller loadings, even up to 30 wt% [7]. Indeed, the incorporation of vermiculite in PA11 results in significant enhancement of some mechanical, thermomechanical, flame retardancy and optical properties due to the reinforcement effect of the high aspect ratio of these nanofillers [18]. Since these relatively new nanocomposites are potentially interesting for various applications (automotive, packaging, others), the knowledge of their resistance to weathering, not only for aesthetic aspects such as yellowing, but also for changes in physical properties such as embrittlement, is an important issue [19]. In this context, many publications dealing with the thermal-oxidation of PA11 nanocomposites are available in the open literature [7, 20-21].

Accordingly, it is reported that the nanocomposites undergo faster degradation, mainly due to the catalytic effect of the iron ions contained in the silicate filler. However, there is rather limited literature on photo-oxidative degradation of PA11/vermiculite nanocomposites, although photo-oxidation is considered as one of the primary sources of damage to polymer materials [9].

In this work, the objective was to investigate the photooxidation under accelerated UV test of PA11/unmodified vermiculite nanocomposite films through changes in the chemical structure, morphology and the optical and thermal properties. The unmodified vermiculite nanoclay (UVMC) thermally expanded, was incorporated at 5 wt. % into PA11. The degradation was evaluated by tracking carbonyl, yellowing and crystalline indexes in comparison with those of neat PA11. Moreover, the stability of the samples was also determined by measuring the onset oxidation temperature (OOT).

2. Experimental

2.1. Materials used

PA11 was provided in powder form by Arkema (France) under the grade Rilsan ES Naturelle. According to the manufacturer, this grade is colorless and free of any other additives. The resin is mainly used in metal coating by electro spraying (ES). Further, the polymer has a moderate viscosity with a melting point of 186 °C. According to the manufacturer, this grade is the only high performance polymer which is 100% based on renewable resources.

The starting vermiculite (UVMC), grade Superfine (1 mm) from Palabora mining (South Africa) was obtained from Mandoval Vermiculite Company (South Africa). Vermiculite is flake-like and it is a mica-type silicate, which belongs to the general family of 2:1 layered silicates. Each layer consists of octahedral coordinated cations (typically Mg, Al and Fe) sandwiched by tetrahedral coordinated cations (typically Si and Al). According to Muiambo et

al. [22], Palabora vermiculite has the following structural formula: $0.60(Mg_{2.60}Fe^{2+}_{0.60})[Si_{3.2}Al_{0.78}Fe^{3+}_{0.02}]O_{10}(OH)_2K^{+}_{0.49}$ + $(0.40)(Mg_{2.60}Fe^{2+}_{0.60})[Si_{3.2}Al_{0.78}Fe^{3+}_{0.02}]O_{10}(OH)_2Mg^{2+}_{0.20}.nH_2O$

The thermal exfoliation of vermiculite was achieved by exposing the material for 5 min to the temperature of 700°C in a convection oven. Then, the exfoliation into submicronic and nanoflakes was accomplished by sonication using high power ultrasound. The detailed procedure of UVMC exfoliation is clearly described by Macheca et al. [7].

2.2. Sample preparation

UVMC was melt-compounded with PA11 at filler content of 5 wt. %. For comparison, the neat polymer was also subjected to the same processing conditions. The compounding process was carried out using a Nanjing Only Extrusion Machinery Co. Ltd, (Model TE-30/600-11-40) co-rotating twin-screw laboratory extruder (diameter = 30.0 mm, L/D = 40:1) operating at a feed rate of 2 kg h^{-1}. The barrel temperature profile ranged from 70 to 230°C and the screw speed was set at 27 rpm. The extruded materials passed through a cooling water bath system, pelletized, and finally dried in a convection oven at 40°C for 4 days.

Film samples were prepared by using a single screw extruder of Model Collin CR 72T, Esberg, Germany. Prior to processing, the pellets of both neat PA11 and PA11 nanocomposite obtained from the twin-screw extruder were again dried in an oven at 105°C for 24 h. The single extruder has, as terminal, a calendar characterized by two counter-rotating cylinders that allow the film passing through them still in the plastic state and a third cylinder to direct the output material up to the collecting cylinder. The extrusion was conducted at the following temperatures: 169/215/230°C along the barrel. The screw speed was 35 rpm. The average film thickness was 60±5 μm.

2.3. Accelerated UV test

A UV weathering tester made by the Q-Panel Company (Cleveland, Ohio) and equipped with 6 UVA-340 lamps was used to accelerate the photo-aging of the film samples. These lamps are the best available simulation of sunlight in the short wavelength region between 295 and 365 nm. Film sheets with dimensions of 100x70 mm were cut from neat PA11 and PA11/UMVC nanocomposite and exposed to UV light at 63°C. Specimens were taken out at regular intervals for testing up to 600h.

2.4. Characterization

2.4.1. Fourier transform infrared (FTIR) spectroscopy

Infrared spectra of PA11 and PA11/UVMC nanocomposite samples were recorded on a PerkinElmer spectrum 100 FTIR spectrophotometer at a resolution of 4 cm^{-1} and represent averages of 16 scans. All spectra were recorded in absorbance mode in the 4000-600 cm^{-1} region. The absorption band at 1690 cm^{-1} was used to evaluate the formation rate of imide groups at different photooxidation times. The carbonyl index was obtained by calculating the change in carbonyl absorption band at 1690 cm^{-1} from the FTIR spectra at different exposure times, using the spectrum of the starting non-oxidized materials as reference. All absorbencies were normalized by the film thickness according to eq. (1) [14]:

$$\Delta Abs_{1690cm\text{-}1} = (Abs_{1690cm\text{-}1}t - Abs_{1690cm\text{-}1}t_0)/d \qquad \textbf{(1)}$$

Where, $Abs_{1690\ cm\text{-}1}t$ is the measured absorbance at 1690 cm^{-1} from the FTIR spectrum at a certain exposure time, $Abs_{1690\ cm\text{-}1}t_0$ is the measured absorbance at 1690 cm^{-1} from the FTIR spectrum before exposure and d is the film thickness in microns. An average of three replicates was used for each measurement. For comparison of the FTIR spectra of neat PA11 and PA11/UVMC nanocomposite, a calibration accounting for the small variations of thickness (d,

in μm) and also the nanofiller content was performed using the band at 2853 cm^{-1} (υ(C-H) characteristic vibration stretching band of PA11) [23].

2.4.2. Ultraviolet-visible (UV-visible) spectroscopy

To monitor the discoloration of PA11 and PA11/UVMC nanocomposite films under accelerated UV test, UV spectra were recorded with a PerkinElmer spectrophotometer Lambda 750S, equipped with an integrating sphere preventing the scattered light of the films with a resolution of 2 nm and sampling range of 0.5 nm. A large absorption band displaying a maximum at λ_{max} = 275 nm and extending up to 350 nm grows during exposure. The use of the absorbance change at λ_{max} = 275 nm is justified by its higher sensitivity as long as its optical density remains below 1.4. The absorbance at λ_{max} = 275 nm corresponds to a shoulder that comes out at the initial stages of UV irradiation of the samples and grows during photooxidation process. This shoulder can be taken arbitrarily as a relevant yellowing index, which is defined by eq. (2) [8]:

$$\Delta Abs_{275nm} = Abs_{275nm}t - Abs_{275\,nm}t_0 \qquad \textbf{(2)}$$

Where, $Abs_{275\,nm}t_0$ is the absorbance before exposure and $Abs_{275nm}t$ is the absorbance at a given exposure time. All absorbencies were normalized by the film thickness. An average of three replicates was used for each measurement.

2.4.3. Differential scanning calorimetry (DSC)

Thermal characteristics of neat PA11 and PA11 nanocomposite were determined by DSC (DSC1 Star System-Mettler Toledo) under nitrogen flow (80 mL min^{-1}). Samples of an average weight of 5 mg were crimp-sealed in aluminum crucibles and heated from 30 to 220 °C at a heating rate of 10°C min^{-1} (first heating scan), equilibrated at 220 °C for 5 min, cooled at 10 °C min^{-1} to 30°C, equilibrated at 30 °C for 5 min, and then heated again to 220 °C at 10 °C

min^{-1} (second heating scan). The first heating scan was performed to eliminate the sample's thermal history. The crystallization temperature (T_c), melting temperature (T_m), crystallization enthalpy (ΔH_c) and melting enthalpy (ΔH_m) were determined from DSC thermograms. The degree of crystallinity (X_c) was calculated using eq. (3):

$$Xc = \frac{\Delta Hm}{\Delta H°m(1-wt)} x100 \qquad \textbf{(3)}$$

Where ΔH_m is the melting enthalpy, ΔH_m^0, the melting enthalpy for 100% crystalline sample ($\Delta H_m^0 = 226.4\ J/g$) [16] and wt is the clay weight fraction in the nanocomposite.

The determination of onset oxidation temperature (OOT) is widely used method in the thermal analysis of polymers to evaluate their stability under oxidative conditions [17]. OOT was evaluated in accordance to the following procedure: the sample was heated up continuously (i.e. 10°C min^{-1}) under air flow. OOT was determined as that point in the thermogram where the onset of the decomposition signal resulted. OOT is usually more clearly pronounced as the onset time in oxidation induction time (OIT) measurements.

Scanning electron microscopy (SEM)

Morphological surface changes due to aging of neat PA11 and PA11/UVMC nanocomposite were observed using a Jeol JSM-6031 scanning electron microscope to examine the film samples before exposure and after 600 h under accelerated UV test. Prior to observation, the surface of the film samples was coated with a thin carbon layer by means of a polaron sputtering apparatus.

Transmission electron microscopy (TEM)

The dispersion of UVMC in PA11 was observed by a transmission electron microscope (TEM) of a Model JEM-1200EX, JEOL, Tokyo, Japan (cold field emission gun 100 kV, point to point resolution = 0.23 nm). Prior to analysis, the sample was prepared using an ultramicrotome Leica UC7 equipped with a diamond knife. The ultrathin section was cut at room temperature and under dry conditions and then transferred onto 300 mesh Cu grids coated with a lacy carbon film.

3. Results and discussion

3.1. Nanocomposite morphology

The TEM micrographs offer the most direct observation of the dispersion of UMVC particles in PA11 nanocomposite. In this regard, **Figure 1a** and **b** show the TEM micrographs of PA11/UVMC (5 wt. %) nanocomposite before exposure at 100 and 200 nm scales, respectively. In **Figure 1a** relative to 100 nm scale, the vermiculite layers appear as dark-grey lines. In addition, sheet-like patterns or layers are observed with different orientations indicating that the clay is exfoliated in the nanocomposite. In **Figure 1b**, the vermiculite is visible in black shadow randomly oriented into fine layers and some stacks of the unmodified vermiculite are observed as thick dark lines, with a layer length higher than 200 nm as reported by Woo et al. [24]. Based on these observations, PA11/UMVC nanocomposite exhibits an intercalated-exfoliated structure. This is also an indication that better nano-dispersion has been obtained with UVMC in PA11 matrix.

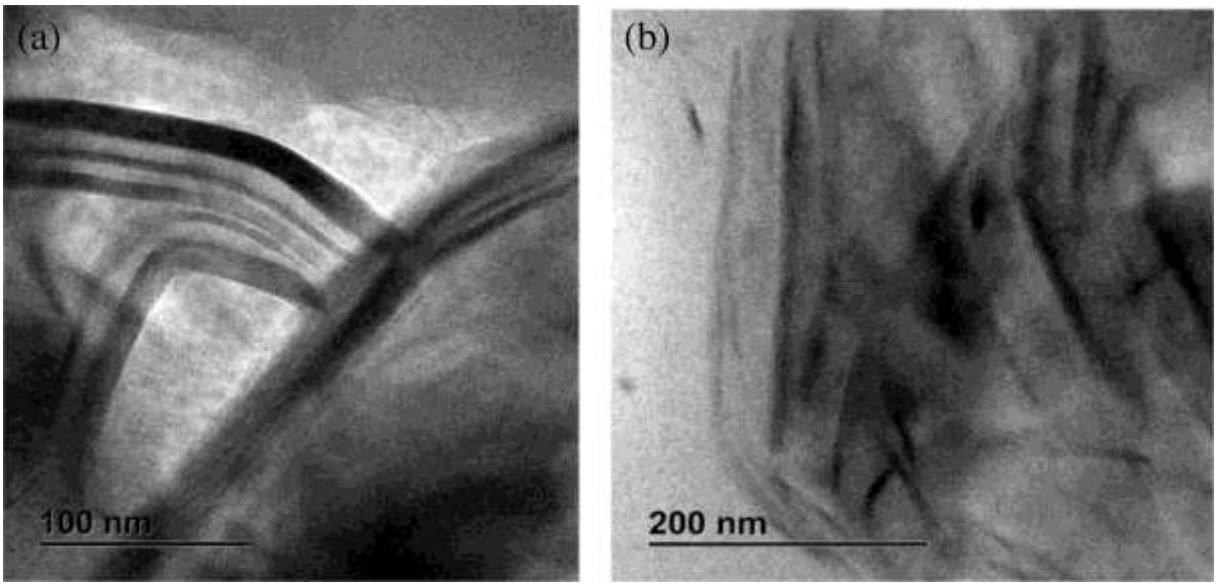

Figure 1. TEM images of PA11/UVMC (5 wt%) nanocomposite at a scale of 100 nm (a) and 200 nm (b).

3.2. FT-IR analysis

Figure 2 shows the FTIR spectra of PA11 recorded before exposure and at 240 and 600h in the 1800 – 1660 cm^{-1} region. From **Figure 2**, the FTIR spectra of neat PA11 exhibit a large absorption band in the region 1800 – 1660 cm^{-1}, whose intensity increases with exposure time, overlapping various carbonyl products. However, two noticeable absorption bands are emerging from this, and growing with UV exposure time. These previously identified absorption bands located at 1736 and 1690 cm^{-1} are assigned to imide groups, which are the main photo-oxidation products [25-27]. The intensity of these peaks is directly related to the degree of photooxidation of the PA11 matrix. Further, a small absorption band located at λ_{max} = 1713 cm^{-1} is also noticed, especially at longer exposure time, corresponding to carboxylic acid groups [27,28]. Accordingly, the photooxidation mechanism of PA11 leads to the formation of imide products resulting from the photochemical decomposition of hydroperoxides through the homolysis of the peroxide bonds [26]. The recombination of the radicals formed leads to imide groups. On the other hand, the formation of carboxylic acid groups absorbing at λ_{max} = 1713 cm^{-1} in photo-oxidation of PA11 results from the hydrolysis of imide groups with

water that is formed in situ in close vicinity of these groups [26]. Similar conclusions can be drawn from the PA11/UVMC sample. This is clearly shown in **Figure 3**, related to the FTIR spectra of PA11/UVMC (5 wt. %) nanocomposite. Indeed, comparison of the different FTIR spectra of the PA11 nanocomposite with that of neat PA11 indicates no shift of the absorption band position in presence of UVMC. This suggests that the photooxidation mechanism of PA11 is not modified in the presence of UVMC, confirming the data previously reported in literature [29,30]. The accumulation of imide groups with exposure time, as a result of hydroperoxide decomposition of neat PA11 and PA11/UVMC nanocomposite, was monitored by observing the change in the absorption band at λ_{max} = 1690 cm^{-1}. **Figure 4** compares the photo-oxidation rates through the evolution of $\Delta Abs_{1690\ cm^{-1}}$ as a function of exposure time for neat PA11 and PA11/UMVC nanocomposite. The plots show the absence of any induction period for carbonyl groups. According to Richaud et al. [31], in aliphatic amide oxidation, α-amino methylenes are more reactive than the other methylene species, so that they firstly undergo oxygen attack. This leads to formation of α-amino hydroperoxides, which are strongly destabilized by the inductive effect of the neighboring nitrogen atom. The decomposition of α-amino hydroperoxides by unimolecular mode is responsible for the absence of an induction period, even at low temperatures. Furthermore, it is clearly observed in **Figure 4** that at the initial stages of exposure until almost 240 h, all irradiated samples exhibit a rapid increase in the kinetic curves of $\Delta Abs_{1690\ cm^{-1}}$ with a slope related to the auto-oxidation rate. However beyond 240 h, there is a slowing of the photooxidation rate. **Figure 4** shows also that the photooxidation rate of PA11 is faster than that of PA11/UMVC nanocomposite, although the curves display the same trend, i.e. a hyperbolic shape. Indeed, UVMC exhibits clearly the ability to slow down the photo-oxidation rate of PA11, despite it contains iron ions, acting as decomposers of the hydroperoxides through redox reactions as reported in literature [32]. One plausible explanation of this surprising result may be the presence of vermiculite flakes at the surface of

the film sample, leading to the formation of a layer slowing down the oxygen diffusion in the amorphous surface of PA11, thus providing oxygen barrier effects. As a result, the primary photo-oxidation products are reduced. Another suggestion is related to the nanocomposite morphology through intercalated-exfoliated structure, which may increase the diffusion time of O_2 in the polymer matrix.

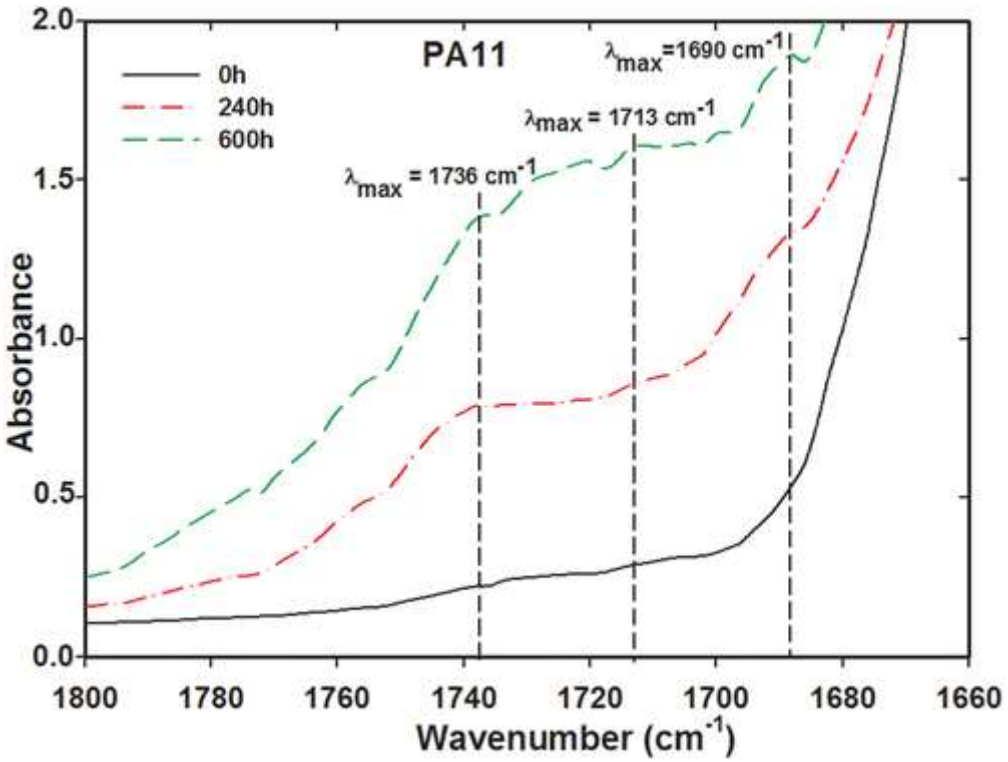

Figure 2. FTIR spectra of neat PA11 recorded in the carbonyl region before exposure and at 240 and 600 h.

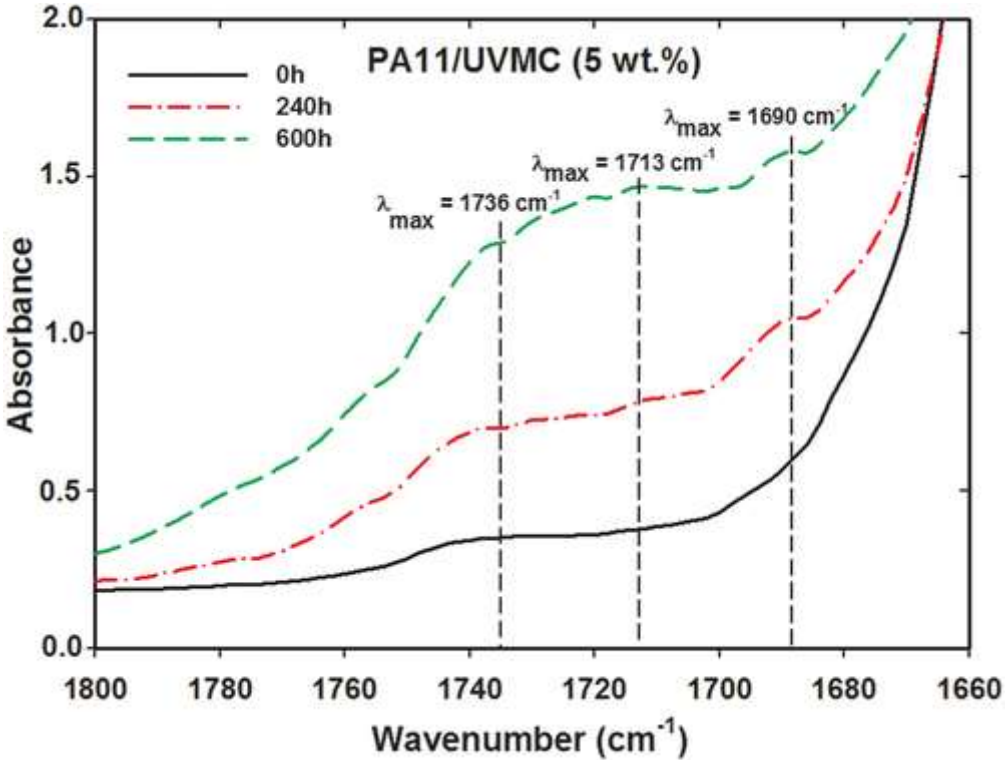

Figure 3. FTIR spectra of PA11-UVMC (5 wt%) nanocomposite recorded in the carbonyl region before exposure and at 240 and 600 h.

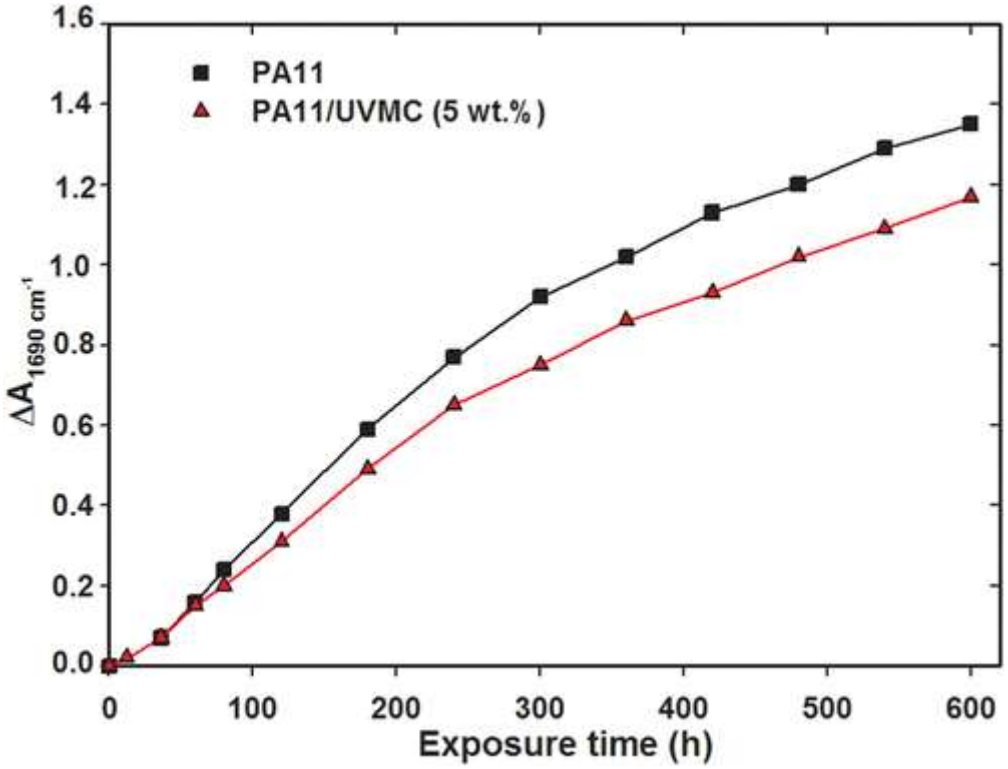

Figure 4. Carbonyl index evolution as a function of exposure time for neat PA 11 and PA 11/UVMC (5 wt%) nanocomposite.

3.3. Evaluation of yellowing

A change in optical properties like discoloration is a common consequence of oxidation of polyamides [33]. This color change restrains the use of such polymer materials in applications where clarity is requested (e.g. food packaging materials) [34]. In addition, changes in appearance may also affect the aesthetic value of objects, as well as their mechanical stability [35]. In this study, discoloration was evaluated through determination of the yellowing index (YI) by UV-vis spectrophotometry. **Figure 5** and **6** shows UV-vis spectra for neat PA11 and PA11/UVMC (5 wt. %), respectively recorded in the range of 230 – 400 nm before exposure and at 240 and 600h. In both figures, the UV-vis spectra related to the reference samples display no absorption band in the range of 230 – 400 nm. However after exposure of the film samples to accelerated photo-oxidation, the UV-vis spectra of neat PA11 and PA11/UVMC nanocomposite exhibit a significant modification with respect to the reference ones through the formation of a large absorption band centered at maximum wavelength λ_{max} = 275 nm, whose intensity increases steadily with increasing the exposure time up to 600 h. Moreover, the value of the absorption band at λ_{max} = 275 nm observed in irradiated PA11 and PA11/UVMC nanocomposite samples is close to that reported by Fromageot et al. [33], indicating the formation of an absorption band centered at 280 nm in a thermo-oxidized PA11 film at 90°C. Tang et al. [36] observed an absorption band at 290 nm in the UV spectra of irradiated PA11 film in a SEPAP 254 device at almost 30°C, whose intensity increases in the initial exposure time before reaching a stationary state. The authors attributed the absorption band at λ_{max} ~ 290 nm to aldehyde groups, which can accumulate at 30°C resulting from the excitation of imide groups at wavelengths longer than 300 nm. The aldehyde groups are photo-oxidized to acidic compounds. The latter can be observed at λ_{max} = 1713 cm^{-1} in the FTIR spectra of both irradiated PA11 and PA11/UVMC nanocomposite. Although, the nature of the oxidized groups responsible for the discoloration of PA 11 is still in debate [31], the UV

absorbing products are likely attributed to the formation of conjugated carbonyls resulting from the crotonization of aldehydes [27,28].

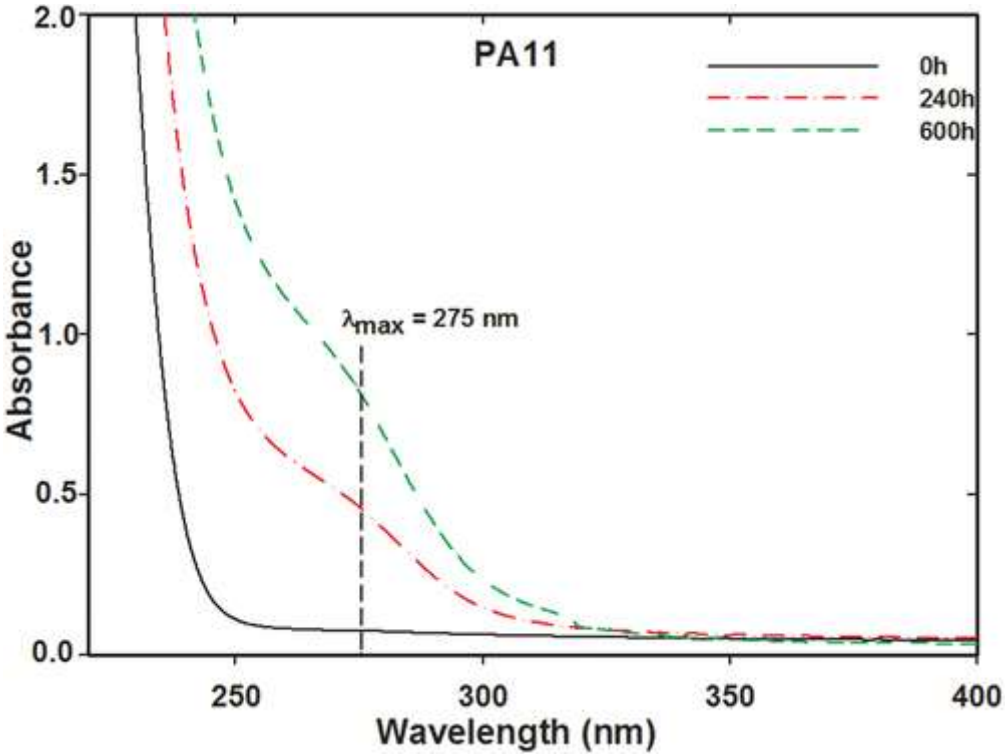

Figure 5. UV–vis spectra of neat PA11 recorded in the range 230–400 nm before exposure and at 240 and 600 h.

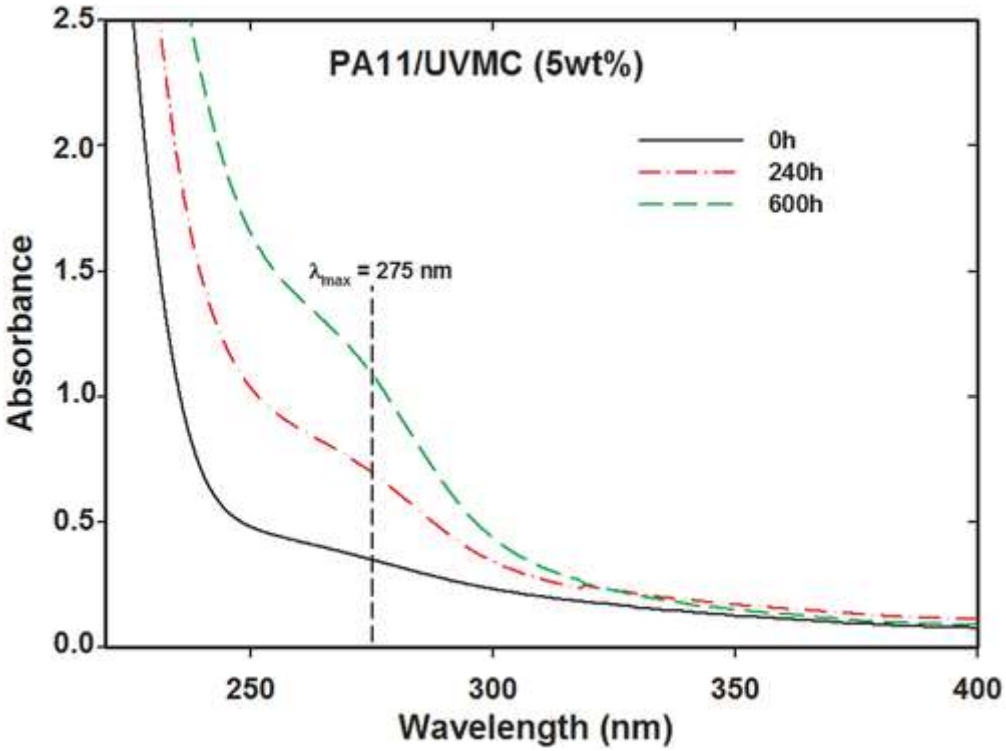

Figure 6. UV–vis spectra of PA11/UMVC (5 wt%) nanocomposite recorded in the range 230–400 nm before exposure and at 240 and 600 h.

Figure 7 shows the kinetic curves of the yellowing index (YI) for the neat PA11 and PA11/UVMC nanocomposite samples up to 600h. A fast growth of the YI at the beginning of exposure up to almost 200h, before slowing slightly, is observed. Furthermore, the kinetic curves display any induction period. It is further noted that the PA11/UVMC nanocomposite shows relatively lower YI kinetics than the neat PA11, which is consistent with the data obtained by FTIR analysis. According to Fromageot et al. [33], the increase in absorption of UV light by species can be explained by a new crotonization reaction of aldehydes of the polymer matrix itself. It is assumed that the chain scission mechanism is prevalent after longer exposure time. This leads to shorter polymer chains with subsequent increase in the aldehyde crotonization.

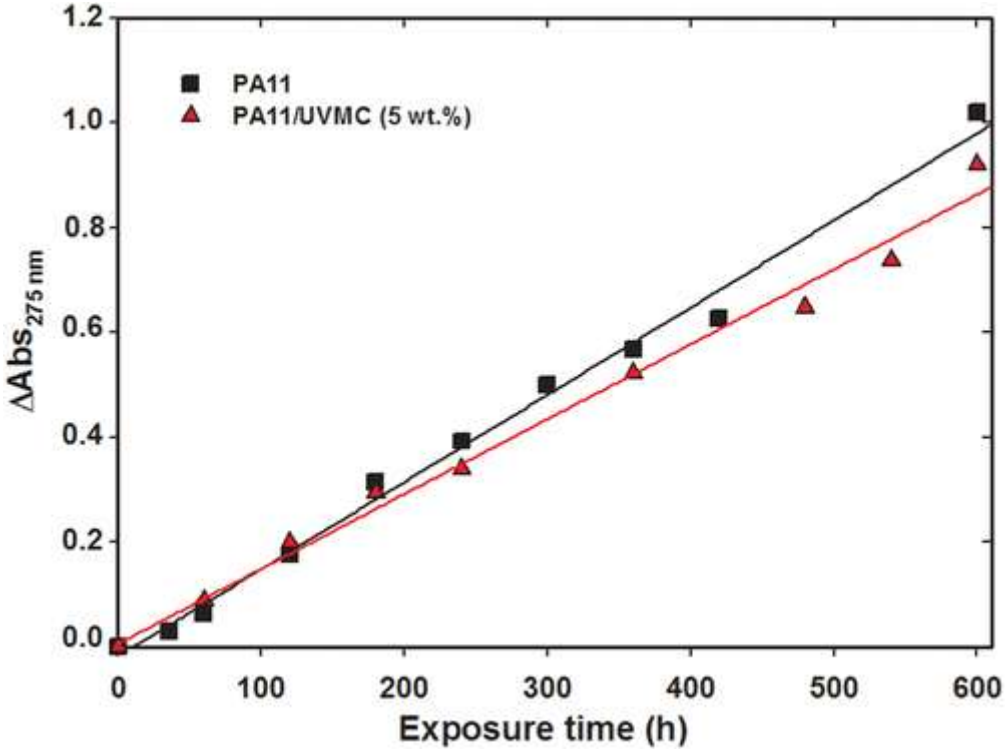

Figure 7. YI evolution as a function of exposure time for neat PA 11 and PA 11/UVMC (5 wt%) nanocomposite.

Figure 8 shows the relationship between UV absorbing compounds at 275 nm and the FTIR absorption of the imide groups at 1690 cm^{-1} for both PA11 and PA11/UVMC nanocomposite. **Figure 8** cannot be used for an accurate measurement of the process of polymer photo-

oxidation. It only shows the possibility to correlate the formation of absorbing species at 275 nm to that of amide groups along the photo-oxidation process of neat PA 11 compared to PA11/UVMC.

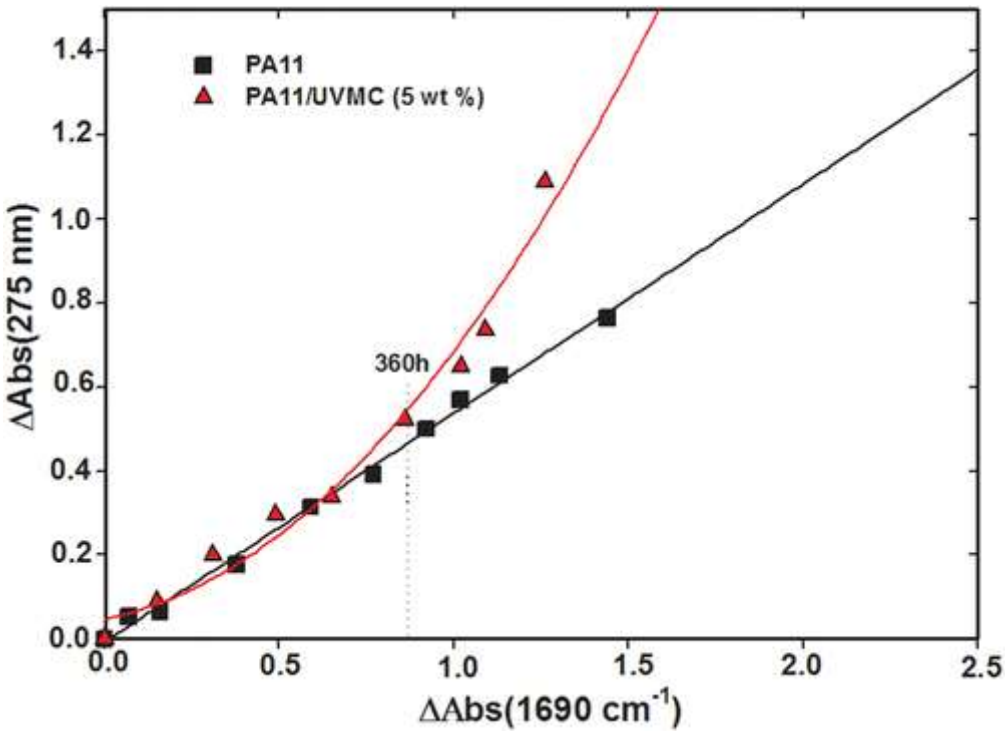

Figure 8. YI versus carbonyl index for neat PA 11 and PA 11/UVMC (5 wt%) nanocomposite.

It is observed that the formation of absorbing compounds in the neat PA 11 increases almost linearly with imide groups. This indicates that the conversion rate of imide groups into UV absorbing products is comparable along the photo-oxidation process. For the PA11/UVMC nanocomposite sample, **Figure 8** shows that up to approximately 240h of exposure, the conversion rate of imide groups to UV absorbing species is comparable to that of neat PA11 following almost the same linear function. However above 240h, there is a deviation from the linearity indicating a fast increase in the absorbing UV compounds, which becomes much higher at longer irradiation time.

3.4. DSC analysis

The DSC thermograms displaying the thermal characteristics for neat PA11 before exposure and after 600 h are shown in **Figure 9**. From **Figure 9**, the presence of a double melting peak before exposure is observed. Similar behaviour is also noticed for PA11/UVMC nanocomposite (DSC thermograms not shown). The presence of a double melting peak in both PA11 and PA11/UVMC nanocomposite is assigned to two forms of crystal or one type of crystal exhibiting different sizes or degrees of perfection [4]. As a matter of fact, Stoclet et al. [5] reported that the presence of two melting peaks in PA11 matrix is ascribed to the melting-recrystallization process of the ɣ form into the thermodynamically stable α form. After 600h of exposure, the DSC thermograms of irradiated PA11 clearly show a broadening of the melting peaks with a significant shift toward the lower temperatures, with the effect being less pronounced than the PA11/UVMC nanocomposite sample. Similar behaviour is also observed for the crystallization temperature. Although changes of melting temperature as well as enthalpy result from the occurrence of different simultaneous processes, Mago et al. [6] attributed the decrease of T_m to the formation of small or imperfect crystals which are likely to have a lower melting temperature. The literature also reported that the decrease of T_m may be ascribed to changes in crystallite thickness and its distribution [37]. Furthermore, Cerruti et al. [38] indicated that the formation of less ordered crystallites with an increased surface energy is responsible for the decrease of melting temperature. The authors argued that the oxidative degradation can spread out to the tie molecules connecting the crystallites and the chain folds at crystal surface, leading to imperfection in the crystalline structure. **Table 1** provides the thermal characteristics values of T_m, T_c, ΔH_c, ΔH_m and X_c for the neat PA11 and PA11/UVMC nanocomposite with exposure time. The data show that before exposure, both the high and low melting peaks values of PA11 and PA11/UVMC nanocomposite are very similar. However, a slight increase in the T_c value is observed for the nanocomposite sample compared to that of

neat PA11. Furthermore, a minor change in X_c of neat PA11 after addition of UVMC is also noticed. The slight increase of T_c in PA11/UVMC nanocomposite may be attributed to a small nucleating effect induced by the nanofiller. Indeed, the literature [38] reported that at high filler content, i.e. above 5 wt. %, the amount of clay is sufficient to hinder the chain mobility of the polymer and subsequently results in the delay of crystal growth. With increasing the exposure time, a considerable decrease in T_m and T_c values is observed, being more pronounced at 600h. It can also be noted that PA11/UVMC nanocomposite exhibits the same thermal behaviour as the neat polymer during the course of the photo-oxidation process. DSC data show also a similar trend in the evolution of X_c value with exposure time for both PA11 and the PA11/UVMC nanocomposite. This is characterized by a rapid increase of X_c at the initial stage of exposure reaching a maximum at almost 360h before decreasing noticeably. According to the literature [39], the increase in X_c during the early stages of exposure results from the occurrence of the well-known chemi-crystallization phenomenon due to chain scission mechanism leading to the formation of shorter macromolecular chains. The latter have higher mobility and they are capable to crystallize in the amorphous phase of the polymer. As the exposure time becomes longer, X_c decreases meaning that the photo-oxidation process damagingly affects the crystalline regions as reported by Cerruti et al. [38]. No cross-linking fraction is formed in both aged PA11 and PA11/UVMC samples at 600h of exposure as revealed by the solubility test using m-cresol as the solvent. Thus at longer exposure time, the phenomenon of damaging the crystalline regions is more dominant than the chemi-crystallization phenomenon occurring in the amorphous phase of the polymer. The results also mean that accelerated photo-oxidation promotes the appearance of crystallite defects in PA11, and to a lesser extent in PA11/UVMC nanocomposite, implying changes in their morphologies as a reduction in the crystalline domain. This obviously increases the sensitivity of the materials to further photodegradation.

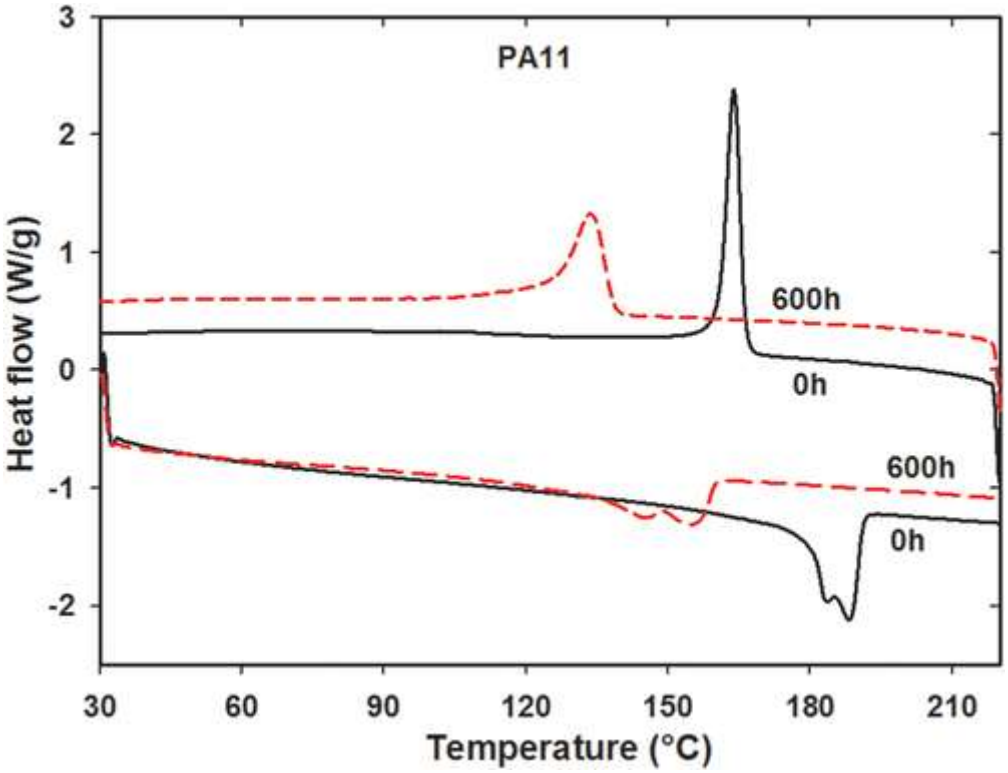

Figure 9. DSC thermograms of neat PA11 before exposure and after 600 h.

Table 1.Variation of thermal characteristics of neat PA11 and PA11/UVMC (5 wt.%) nanocomposite with exposure time.

Samples	Exposure time (h)	T_m(°C)	T_c(°C)	ΔH_m(J/g)	ΔH_c(J/g)	X_c(%)
PA11	0	183–188	164	64	60	33
	120	177–184	164	76	75	39
	240	167–174	156	76	79	39
	360	168–176	157	78	75	40
	600	145–154	134	60	59	31
PA11/UVMC (5 wt%)	0	184–188	166	61	55	31
	120	175–182	164	70	70	36
	240	170–178	159	71	71	36
	360	166–174	156	68	64	35
	600	151–159	141	61	62	31

In order to evaluate the effect of UVMC on the photo-stability of PA11, the onset oxidation temperature (OOT) was monitored by DSC. In this regard, **Figure 10** shows the OOT thermograms of neat PA11 before exposure and after 600h. OOT corresponds to the intersection of the baseline after melting and the slope of the oxidation curve [40]. The OOT value of PA11 is approximately 311°C. After 600h, a noticeable change is observed on the thermogram of PA11, which mainly results in a sharp decrease in the OOT value from roughly 311 to 298°C (13°C lower). **Figure 11** shows the OOT thermograms of PA11/UVMC

nanocomposite before exposure and after 600h. Before exposure, the OOT value is around 315°C, which is higher than that of neat PA11. After 600h, the thermogram of the PA11 nanocomposite shows a decrease in the OOT value from 315 to almost 308°C representing a difference of 7°C. This result clearly indicates that the effect of accelerated photo-oxidation on the OOT is less pronounced for the PA11/UVMC nanocomposite compared to neat PA11. This also means that the nanocomposite sample is more stable than the neat polymer during the course of photooxidation, which is in good agreement with the FTIR and UV spectroscopic data. **Figure 12** shows the variation of OOT with exposure time for both the neat PA11 and PA11/UVMC nanocomposite. An almost linear decrease in the OOT values with exposure time without any induction period is observed for both samples. This decrease may be due probably to the occurrence of chain scission mechanism in the irradiated samples resulting in the decrease in the molar mass [41]. However, it is interesting to note that the rate of variation is lower for the PA11/UVMC nanocomposite sample in comparison to the neat PA11. The rate of decline of OOT indicates the value of -1.2 10^{-2}°C/h for the PA11/UVMC nanocomposite against -2.15 10^{-2}°C/h for PA11. This reinforces the fact that the addition of unmodified vermiculite to PA11 enhances its resistance against accelerated photo-oxidation.

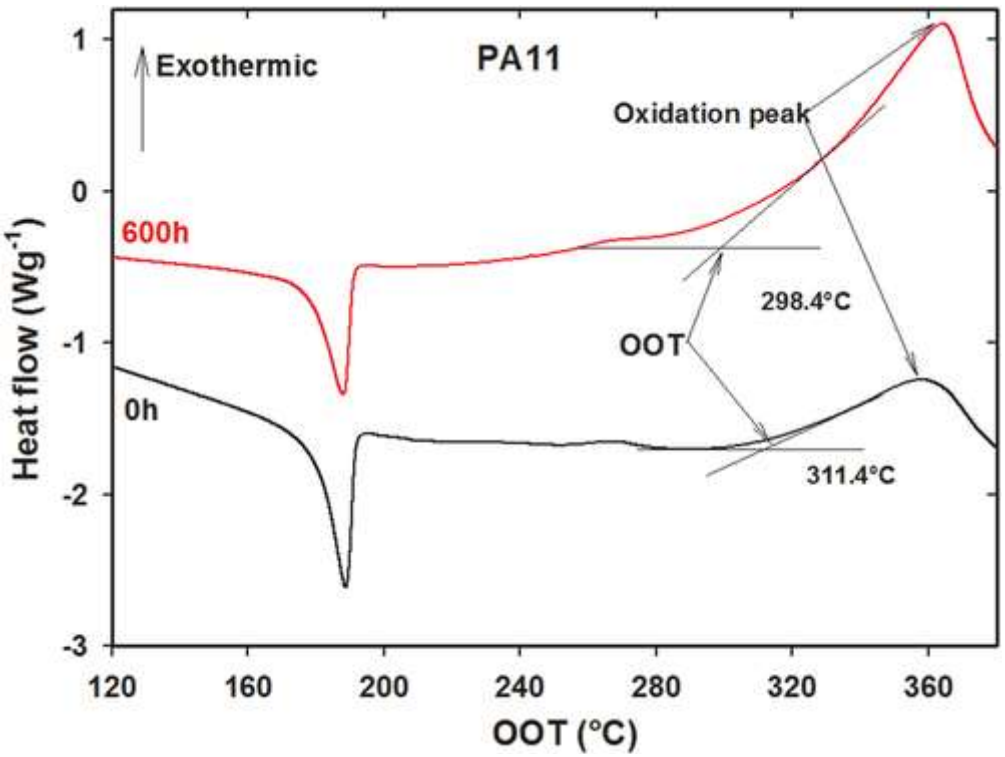

Figure 10. DSC thermograms of OOT of neat PA11 before exposure and after 600 h

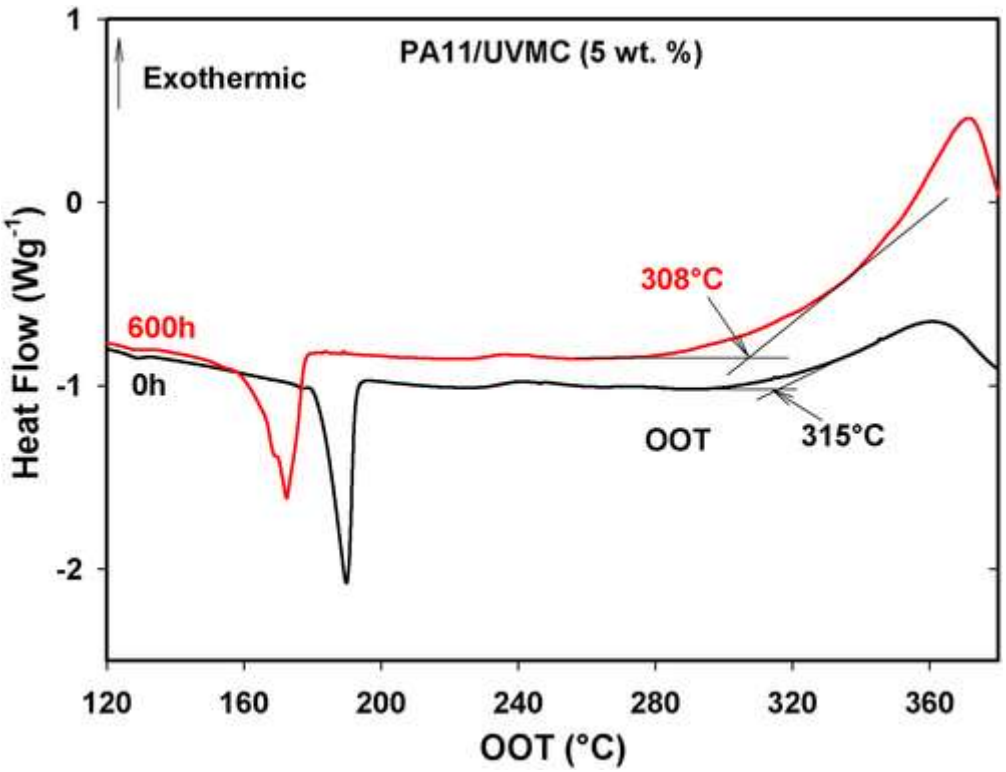

Figure 11. DSC thermograms of OOT of PA11/UVMC (5 wt%) nanocomposite before exposure and after 600 h.

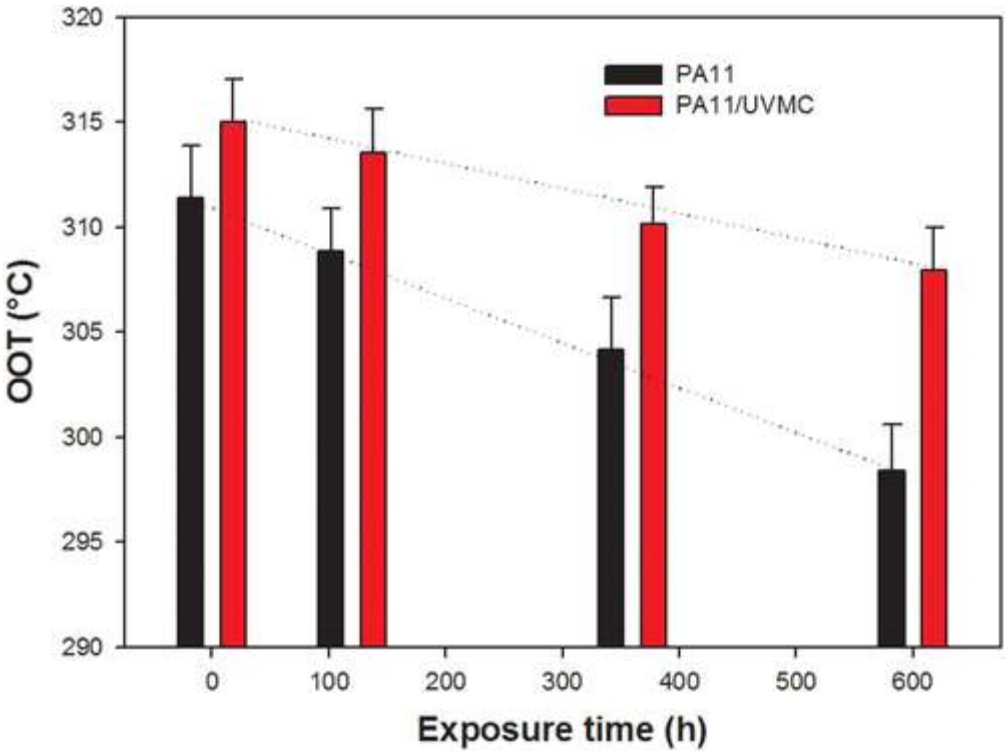

Figure 12. OOT evolution as a function of exposure time for neat PA 11 and PA 11/UVMC (5 wt%) nanocomposite.

3.5. SEM analysis

The occurrence of photo-oxidative degradation considerably affects the surface morphology of irradiated materials, and the changes can be followed by SEM. **Figure 13a** shows the SEM micrograph of the film surface of neat PA11 before exposure, at 40000x magnification. The unexposed surface exhibits a smooth and regular surface morphology, in which crossed lines, probably due to die scratching are observed. The SEM micrograph reveals also that no cracks are visible on the surface. Similar surface morphology is also observed for the PA 11/UVMC nanocomposite sample (not shown here).

However after 600h of exposure, it is observed in both PA11 and PA11/UVMC samples, a considerable surface damage through the appearance of pattern of cracks and voids on the surface as shown in **Figure 13b and c** corresponding to the neat matrix and the nanocomposite, respectively. However, the damage seems to be more severe for the neat PA11 as evidenced by more pronounced surface erosion.

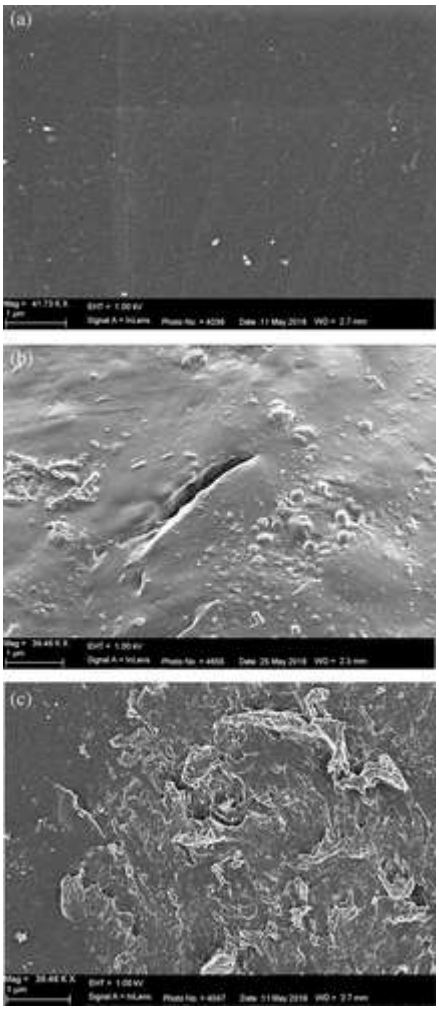

Figure 13. SEM micrograph of the film surface of PA11 before exposure (a) and after 600 h of exposure (b), and of PA11/UVMC (5 wt%) nanocomposite after 600 h of exposure (c) (4,0000×).

Conclusion

Thin films based on PA11 and PA11/UVMC nanocomposite (5 wt. %) were successfully prepared by melt processing. The morphology as characterized by TEM revealed a good intercalation/exfoliation of UVMC into PA 11 matrix. The samples were then subjected to accelerated UV test up to 600h. Our goal was to evaluate the effect of UVMC on the photo-oxidation process of PA11/UVMC nanocomposite under accelerated UV test. It was found that the FTIR spectra of the nanocomposite samples exhibited similar shape in the carbonyl region as those of neat PA11during the course of photo-oxidation process, characterized essentially by the formation of imides and carboxylic acid. However, only the absorption band intensity of the carbonyl groups has changed. Indeed, the FTIR data showed that the carbonyl rate of

PA11/UVMC nanocomposite was lower than that of neat PA11. It was further observed that the yellowing index determined by UV-vis spectroscopy followed a similar trend as the carbonyl index. Additionally, OOT measurements have confirmed the data obtained by FTIR and UV-vis analyzes. The complete set of data clearly showed better photo-stability of the PA11/UVMC nanocomposite over the neat polymer. This was due probably to the accumulation of vermiculite on the film surface leading to the formation of a surface layer acting as oxygen barrier effect, thus reducing the photo-oxidative degradation.

Acknowledgements

M.K. would like to thank the DGRSDT-MESRS (Algeria) for its financial support to carry out this study in the frame of the sabbatical year at the University of Pretoria in South Africa. Many thanks for the Chemical Engineering Department for hosting me and the Laboratory of Microscopic Analysis for SEM and TEM analysis.

References

1. K. Prashantha, M.-F. Lacrampe, and P. Krawczak, *J. Appl. Polym. Sci*., **130**, 313 (2013).

2. M. Sahnoune, M. Kaci, A. Taguet, K. Delbe, S. Mouffok, S. Abdi, J-M. Lopez-Cuesta, and W. W. Focke, *J. Polym. Eng.*, **39**, 25 (2019).

3. A. Hao, I. Wong, H. Wu, B. Lisco, B. Ong, A. Sallean, S. Butler, M. Londa, and J. H. Koo, *J. Mater. Sci*., **50**, 157 (2015).

4. Q. Zhang, M. Yu, and Q. Fu, *Polym. Int.*, **53**, 1941 (2004).

5. G. Stoclet, M. Sclavons, and J. Devaux, *J. Appli. Polym. Sci*., **127**, 4809 (2013).

6. G. Mago, D. M. Kalyon, and F. T. Fisher, *J. Polym. Sci. Part B: Polym. Phys*., **49**, 1311 (2011).

7. A. D. Macheca, W. W. Focke, H. F. Muiambo, and M. Kaci, *Eur. Polym. J*., **74**, 51 (2016).

8. O. Okamba-Diogo, E. Richaud, J. Verdu, F. Fernagut, J. Guilment, and B. Fayolle, *Polym. Degrad. Stab*., **120**, 76 (2015).

9. E. Olewnik-Kruszkowska, *J. Therm. Anal. Calorim*., **119**, 219 (2015).

10. L. Zaidi, M. Kaci, S. Bruzaud, A. Bourmaud, and Y. Grohens, *Polym. Degrad. Stab*., **95**, 1751 (2010).

11. P. K. Annamalai, D. Depan, N. S. Tomer, and R. P. Singh, *Prog. Polym Sci*., **34**, 479 (2009).

12. D. Garcia-Lopez, J. F. Fernandez, J. C. Merino, J. Santaren, and J. M. Pastor, *Comp. Sci. Technol*., **70**, 1429 (2010).

13. S. Kennouche, N. Le Moigne, M. Kaci, J.C. Quantin, A-S. Caro-Bretelle, C. Delaite, and J.-M. Lopez-Cuesta, *Eur. Polym. J*., **75**, 142 (2016).

14. M. Scoponi, S. Cimmino, and M. Kaci, *Polymer*, **41**, 7969 (2000).

15. M. Kaci, T. Sadoun, and S. Cimmino, *Int. J. Polym. Anal. Charact*., **6**, 455 (2001).

16. O. Okamba-Diogo, E. Richaud, J. Verdu, F. Fernagut, J. Guilment, and B. Fayolle, *Polymer*, **82**, 49 (2016).

17. M. Schmid, A. Ritter, and S. Affolter, *J. Therm. Anal. Cal*., **83**, 367(2006).

18. A. D. Macheca, W. Focke, M. Kaci, B. Panampilly, and R. Androsch, *Polym. Eng. Sci.*, **58**, 1746 (2018).

19. E. Hablot, A. Tisserand, M. Bouquey, and L. Averous, *Polym. Degrad. Stab*., **96**, 1097 (2011).

20. G. Filippone, S. C. Carroccio, R. Mendichi, L. Gioiella, and N. Tz. Dintcheva, *Polymer*, **72**, 134 (2015).

21. S. V. Levchik, E. D. Weil, and M. Lewin, *Polym. Int*., **48**, 532 (1999).

22. H. F. Muiambo, W. W. Focke, M. Atanasova, I. van der Whesthuisen, and L. R. Tiedt, *Appli. Clay Sci.*, **50**, 51 (2010).

23. S. Morlat-Therias, E. Fanton , J.L. Gardette , S. Peeterbroeck, M. Alexandre , and P. Dubois, *Polym. Degrad. Stab*., **92**, 1873(2007).

24. E. M. Woo, and A. Auliawan, *Polym. Comp*., **32**, 1916 (2011).

25. D. Fromageot, J. Lemaire, and D. Sallet, *Eur. Polym. J*., **26**, 1321 (1990).

26. A. Roger, D. Sallet, and J. Lemaire, *Macromolecules*, **19**, 579 (1986).

27. O. Okamba-Diogo, E. Richaud, J. Verdu, F. Fernagut, J. Guilment, and B. Fayolle, *Polym. Degrad. Stab*., **108**, 123 (2014).

28. J. Lemaire, J.-L. Gardette, A. Rivaton, and A. Roger, *Polym. Degrad. Stab*., **15**, 1 (1986).

29. G. Filippone, S. C. Carroccio, G. Curcuruto, E. Passaglia, C. Gambarotti, and N. Tz. Dintcheva, *Polymer*, **73**, 102 (2015).

30. J. K. Panday, K. R. Reddy, A. P. Kumar, and R. P. Singh, *Polym. Degrad. Stab*., **88**, 234 (2005).

31. E. Richaud, O. Okamba-Diogo, B. Fayolle, J. Verdu, J. Guilment, and F. Fernagut, *Polym. Degrad. Stab.*, **98**, 1929 (2013).

32. G. Gorrasi, V. Bugatti, M. Ussia, R. Mendichi, D. Zampino, C. Puglisi, and S. C. Carroccio, *Polym. Degrad. Stab*., **152**, 43 (2018).

33. D. Fromageot, and A. Roger, J. Lemaire, *Makromol. Chem*., **170**, 71 (1989).

34. P. Kiliaris, C. D. Papaspyrides, and R. Pfaendner, *Polym. Degrad. Stab*., **94**, 389 (2009).

35. G. Pastorelli, C. Cucci, O. Garcia, G. Piantanida, A. Elnaggar, M. Cassar, and M. Strlič, *Polym. Degrad. Stab*., **107**, 198 (2014).

36. L. Tang, D. Sallet, and J. Lemaire, *Macromolecules*, **15**, 1432 (1982).

37. E. Bilotti, R. Zhang, H. Deng, F. Quero, H. R. Fischer, and T. Peijs, *Comp. Sci. Technol*., **69**, 2587 (2009) .

38. P. Cerruti, M. Lavorgna, C. Carfagna, and L. Nicolais, *Polymer*, **46**, 4571 (2005).

39. O. Okamba-Diogo, E. Richaud, J. Verdu, F. Fernagut, J. Guilment, and B. Fayolle, *Polymer*, **82**, 49 (2016).

40. O. Okamba-Diogo, E. Richaud, J. Verdu, F. Fernagut, J. Guilment, F. Pery, and B. Fayolle, *Polym. Test*., **52**, 63 (2016).

41. V.-M. Archodoulaki, S. Lüftl, and S. Seidler, *Polym. Test*., **25**, 83 (2006).